Regional Studies in Marine Science 46 (2021) 101891

Contents lists available at ScienceDirect

Regional Studies in Marine Science

journal homepage: www.elsevier.com/locate/rsma

The wind-driven response of the Zambezi River plume along the Sofala Bank: A numerical model study

Fialho P.J. Nehama [a,b,*], Chris J.C. Reason [b]

[a] Escola Sup. de Ciências Marinhas e Costeiras, Eduardo Mondlane University, Quelimane, Mozambique
[b] Department of Oceanography, University of Cape Town, Rondebosch 7701, South Africa

ARTICLE INFO

Article history:
Received 15 July 2020
Received in revised form 3 June 2021
Accepted 10 June 2021
Available online 15 June 2021

ABSTRACT

The Zambezi River plume constitutes a sizable feature in the horizontal distribution of both surface salinity and suspended sediments, and it spreads both downstream and upstream, influencing substantially the coastal ecosystems. Here we present the results of several numerical experiments conducted using the Regional Oceanic Modeling System, to investigate the plume's response to impulsive wind forcing. The model uses realistic geometry and bathymetry, as well as constant discharges emanated from three point sources. Different wind directions and magnitudes were explored, including a daily oscillating wind field. In the absence of wind forcing, a modest discharge generates a plume that propagates northeastwards trapped to the coast. A constant wind field can alter the plume shape to become either a "coastal current" or a "large bulge", depending on the predominant wind direction. The "coastal current" characterized by a northeastward (downstream) spreading of the plume reaching up to 180 km was directly related to a downwelling favorable winds. While the "large bulge" characterized by an increased upstream penetration is related to upwelling-favorable winds. Diurnal breezes were effective in transforming the trajectories of surface water particles into ellipsoids, as well as promoting additional mixing of the plume and ambient waters. The realistic wind field can transport plume waters to nearly 120 km downstream, 75 km upstream, and 65 km seaward.

1. Introduction

The Sofala Bank receives freshwater discharged by the Zambezi River, the largest river flowing into the Indian Ocean from Africa. With an annual mean runoff of 224 km^3 yr^{-1}, freshwater from the Zambezi dominates the water masses in the Bank (Sætre and da Silva, 1982; Gammelsrød, 1992; Siddorn et al., 2001; Nehama et al., 2015). The river has a distinctive seasonal variability characterized by a rise phase during September to February (near the end of the rainy season), and a fall phase spanning the months of March to August (dry season). Monthly mean discharges vary between 1600 m^3 s^{-1} in August to 3000 m^3 s^{-1} in February, and the annual distribution features a second peak in July of about 1900 m^3 s^{-1}, a consequence of upstream river regulation (Hoguane, 1997; Beilfuss and dos Santos, 2001). During the period between 1976 and 2007, after major regulatory infrastructures were built along the river course, nearly 42% of daily discharges were in the range 1000 to 2000 m^3 s^{-1}, while discharges beyond 5000 m^3 s^{-1} occurred in 15% of the time.

The hydrodynamics within the Sofala Bank are dominated by the passage of a number of highly variable anticyclonic eddies propagating poleward. These remarkably large features (more than 300 km wide) are formed roughly every 8 weeks (i.e., six or seven eddies per year) in the northern part of the Mozambique Channel, following a pulse in the volume transported westward by the South Equatorial Current (Backeberg and Reason, 2010). The existence of large anticyclonic eddies in the offshore region implies the existence of a modified poleward current along the Mozambique side of the channel. Such currents induce a variety of secondary effects that includes the generation of cyclonic lee eddies, extraction of shelf waters to the mid-channel region, and significant upwelling at the shelf edge (Lutjeharms, 2006; Banas et al., 2009; Li et al., 2015).

The Zambezi River plume constitutes a sizeable feature in the horizontal distribution of both surface salinity (IMR, 1977, 1978a,b) and suspended sediments (Nehama, 2012) in the Sofala Bank. The plume has been observed to spread both downstream (in the direction of propagation of a Kelvin wave) and upstream (Nehama and Reason, 2014). The seaward intrusion of the plume can reach up to 50 km offshore, and is confined to a water column 15 to 30 m deep (Lutjeharms, 2006). According to Mann and Lazier (2006), the seasonally pulsed input of freshwater into the

* Corresponding author at: Escola Sup. de Ciências Marinhas e Costeiras, Eduardo Mondlane University, Quelimane, Mozambique.
E-mail address: fialho.nehama@uem.ac.mz (F.P.J. Nehama).

https://doi.org/10.1016/j.rsma.2021.101891
2352-4855/

coastal ocean influences the secondary production (e.g., shrimp fisheries) of coastal waters.

Buoyant plumes are very sensitive to not only the freshwater inflow, but also ambient currents and wind forcing. For example, Sheng (2001) showed how a coastal jet is able to restrain the seaward expansion of plume waters and the evolution of a plume-jet system into a cyclonic circulation. Xia et al. (2007) investigated the individual and coupled effects of ambient factors on the dispersal of the Cape Fear River plume, and found that the surface distribution of plume waters changes considerably in the presence of winds. They noted that even a moderate wind could fully reverse the buoyant plume (i.e., from southward to northward depending on the wind direction) under average discharges. In a numerical simulation that employed realistic geometry and bathymetry, Pimenta et al. (2005) found that the distribution of low salinity waters was more sensitive to the wind direction, compared to the river outflow variability.

The wind field in the Mozambique Channel is characterized by the predominance of the monsoon regime in the northern and central parts of the channel (down to 20°S), and trade winds in southern part of the channel (Sætre, 1985; Lutjeharms, 2006). According to Collins et al. (2012) the winds are in general weak within the channel with notably great seasonal variability of both magnitude and orientation in the region north of 15°S. The dominant winds in the northern Mozambique Channel are the northwesterlies/westerlies during the northeast monsoon season (austral summer, January–March), and the relatively stronger southeasterlies during the southwest monsoon (June–September). Between 20°S and 25°S, southerly and southeasterly winds dominate, while at the extreme southern part of the channel easterly winds are likely to prevail throughout the year (Sætre, 1985; Collins et al., 2012). In summer, the Inter Tropical Convergence Zone (ITCZ) lies between 15°S and 20°S, having the East African monsoon winds to the north and the trade winds in the south. The ITCZ reaches its southernmost position in the channel (i.e., 18°S) in February allowing the monsoonal winds in the channel to extend to close to that latitude (Jury et al., 1994; Malauene, 2010). In winter, the ITCZ lies well into the Northern Hemisphere and the winds over the channel are southerly or southeasterly. In addition to these seasonal wind patterns, the Zambezi Delta (located between the latitudes 18 and 19°S) and the adjacent coastal sea are influenced by diurnal wind variations, often called the land/sea breezes. According to Tinley (1971), the breezes immediately south of the Zambezi Delta are predominantly southerly during the morning and easterly during the afternoon. The wind speed only exceeds 8 m/s (strong breeze) 10% of the time, and about 65% of the time it is weaker than a light breeze (CFM, 2008).

Coastal buoyant plumes have been well explored in the literature (e.g. Munchow and Garvine (1993), Oey and Mellor (1993), Fong and Geyer (2002), Mestres et al. (2007), Warrick et al. (2004a,b, 2007)). For instance, Munchow and Garvine (1993) used data from moored instruments, drifters, and profiling systems to describe qualitatively the dispersion of buoyant water along the Delaware Coastal current. Fong and Geyer (2002) investigated the dynamics associated with an unforced surface-trapped plume and demonstrated the consequences of an ambient current on the freshwater transport. Through the combination of in situ observations and satellite remote sensing, Warrick et al. (2004b, 2007)), and Warrick and Stevens (2011) investigated the hydrodynamic forces influencing the spreading of brackish buoyant water. Despite its considerable dimensions and strong influence on the coastal ecosystems along the Sofala Bank (Sætre, 1985; Lutjeharms, 2006; Nehama et al., 2015), little is known about the variability of the Zambezi River plume or the response of the plume to its dynamical forcing.

In this study, the Regional Ocean Model System (ROMS) is used to simulate the Zambezi River plume behavior under the action of impulsive idealized winds, using realistic geometry and bathymetry. Thus, the study substantially extends the simplest model of Nehama and Reason (2015) that used a rectangular channel domain and an idealized forcing with a single river mouth. Here, the influence of several mouths in the Zambezi delta on the plume is considered.

2. ROMS configuration for Sofala Bank

2.1. Model configuration, domain, and boundary conditions

ROMS is a three-dimensional, free-surface, terrain-following model that uses high-order numerical schemes, and the conservative and constancy preserving barotropic/baroclinic coupling to generate accurate solutions, while keeping the computational costs as reasonable as possible for today's standards (Shchepetkin and McWilliams, 2005). The model solves the momentum and transport equations discretized in a three-dimensional framework. The model equations are expressed according to the well-documented Boussinesq approximation. A third-order upstream biased advection–diffusion scheme is used for the momentum equations, and a fourth-order centered scheme the transport of tracers (i.e., salinity and temperature).

The lateral mixing of both momentum and tracers is performed using the Laplacian Smagorinsky scheme applied on the iso-sigma levels. The constant in the Smagorinsky formulation of diffusion was taken to be $Ca = 0.1$ and the background horizontal viscosity and diffusivity coefficients were both set to 50 $m^2\ s^{-1}$. Values of the latter coefficients used in other modeling studies were in general much smaller, however, they resulted in numerical instabilities and model crash due to infinitely large/small mechanical energy, when used with the current model configuration.

Vertical mixing is achieved through the K-Profile Parameterization (KPP), which was first proposed by Large et al. (1994) and later amended and made suitable for shallow water systems by Durski et al. (2004). The KPP mixing formulation works in a way to match separate parameterizations for the surface layer, the ocean interior, and the bottom layer. At the surface layer, the viscosities and diffusivities are determined as functions of the product of a length scale (from the boundary layer similarity theory), a turbulent velocity scale, and a shape function (Durski et al., 2004). At the ocean interior, mixing through this scheme accounts for the effects of shear mixing and internal wave-generated mixing, and is achieved through the gradient Richardson number formulation. At the bottom layer, the mixing formulation is similar to that applied at the surface, with small but important amendments. The performance of the KPP scheme has been evaluated in Durski et al. (2004) for three different model setups (including a two-dimensional coastal upwelling), and it was compared with other mixing schemes in Li et al. (2001, 2005). The results indicated that the KPP scheme performed better than the other available schemes (i.e., second-order turbulence models including the classic formulation of Mellor-Yamada). Similar configurations of ROMS have showed to perform fairly well in the simulation of river plumes both in highly idealized (Hetland, 2005) and realistic (Li et al., 2005) cases.

The model domain comprises the region bounded by 15°–22°S and 34°–40°E (Fig. 1). It is divided into a 4.2 by 4.2 km uniform grid and features a coastal wall 3 m deep on the northwestern side (i.e., along the coast); The topography for this region was produced with a bilinear interpolation of the 1 arc-minute General Bathymetric Chart of the Oceans (GEBCO) product, available online at http://www.gebco.net. The model uses sigma coordinates for the vertical dimension, and 20 sigma levels with the resolution focused near to the surface, which translates into an average of

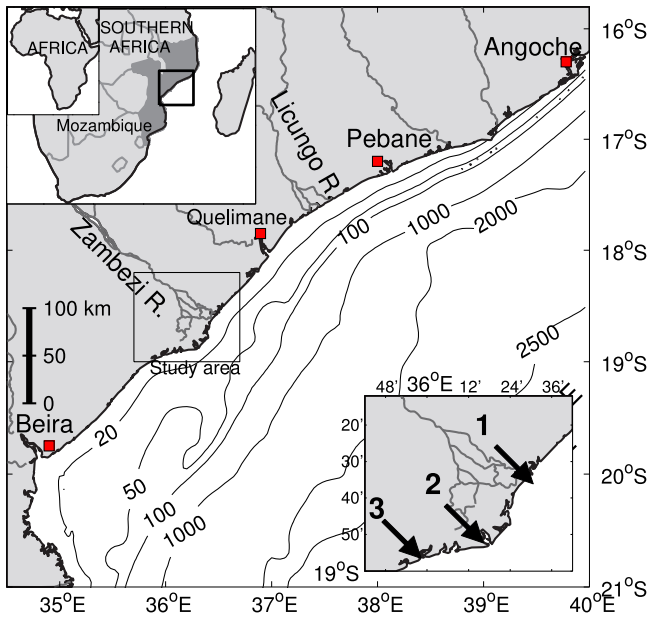

Fig. 1. Bathymetry of the Sofala Bank, extracted from the Gebco1 dataset, which has a spatial resolution of 1 arc-minute re-sampled at 4.2 km resolution, and filtered using the algorithm in the ROMSTOOLS package.

1.1 m of vertical resolution within the plume reach. Since the model does not have wetting and drying cells, a minimum depth of three meters was set at the coast (using as sigma-coordinate stretching parameters $\theta_b = 0.1$, $\theta_s = 3$, and hc=3 m), which overrides the minimum in the detailed realistic bathymetry. The Orlanski radiation conditions were applied to all variables at the open boundaries (i.e., southern and eastern), with an additional volume conservation enforcement, which precludes the reduction in mass volume in the whole domain by integrating the volume transport leaving the domain from a particular boundary and compensating for it at the other open boundary. The conditions imposed at the free surface include a flux of momentum (i.e., wind stress) and no flux of heat and salt. At the bottom, no flux of heat or salt is allowed, and the model uses a logarithmic profile at the lowest grid-point and a specific roughness height (z_0 set to 10 cm), to compute the typical stress condition for the bottom boundary layer. The drag coefficient is given by,

$$C_d = k^2 \left(\ln \frac{z_b}{z_0} \right)$$

Where k is the vonKarman's constant, and z_b is the distance from the seafloor to the bottom grid point. This formulation combined with the above choice of sigma-coordinate parameters results in a constant bottom stress along the river member and a variable stress in the coastal ocean adjacent to the delta. A minimum bottom drag coefficient of $C_{d,min} = 0.001$ is applied to prevent the law-of-the-wall to extend indefinitely, and the maximum drag coefficient allowed was arbitrarily set to $C_{d,max=0.0045}$. The model uses an analytical parameterization for the surface flux of momentum, using Eqs. (1) and (2), and Table 2 presented in Section 3. Given the lack of locally measured wind fields, the direction and magnitude of winds, whenever necessary, were chosen to match the averaged wind conditions during 2000 and 2008, extracted from the QuikSCAT dataset for the 2° by 2° degree box centered at the Zambezi delta.

2.2. Plume initialization

Initially, the ocean is at rest and homogeneous, with salinity and temperature set to 35.5 psu and 29 °C, respectively. The model is forced with a constant volume of brackish water introduced at the three point sources indicated by the numbers over land around the Zambezi River delta in Fig. 1. The actual position of the sources in the numerical grid was set to as close as possible to the coastline, since the constraints imposed by our choice of advection and diffusion schemes implied that sources located very close to the boundary would result in numerical instabilities followed by model crash. By these means, the river outflow was parameterized as a constant volume of water having salinity 20.5 psu and temperature 29 °C. Here, the salinity at the buoyancy source was chosen to match the historical minimum from hydrographic surface data recorded at point source #3 (IMR, 1978b) and is used simply to reproduce the characteristic plume features of the region (Nehama and Reason, 2015). For simplicity, temperature at the source is kept constant. The mass transport at each source was distributed uniformly throughout the water column, and the barotropic velocity was set by ratio of discharge rate to the cross-sectional area. The outflow orientation was chosen to be along the west–east direction, which differs to some degree from the realistic outflow orientation indicated by the arrows in Fig. 1. This choice of outflow orientation might introduce inaccuracies other than those discussed by Garvine (2001) in the nearshore fluxes of plume waters. However, since this model does not consider a river member or estuary, whereby the freshwater is discharged into the coastal sea, and instead brackish water is released directly in the coastal sea, the chosen orientation is likely to have a minor effect on the nearshore dynamics away from the point sources. Additionally, the model configuration employed here avoids the complications that emerge after the freshwater meets the salty ambient water as discussed by Avicola and Huq (2003). The discharge rate increases linearly from nil at time $t = 0$ to a maximum value at time $t = 2\pi/f$. Once the first inertial period is reached, the discharge is set constant throughout the simulation.

2.2.1. Outlet geometry

Before attempting to produce an initial plume upon which the response to wind forcing is analyzed, it seemed instructive to evaluate the impact of outlet geometry. That is, whether a single source or multiple sources should be used, since the freshwater from the Zambezi River in the real system enters the ocean through an extensive delta, with three major branches and a number of small outlets. The distance between the main outlets (i.e., arrows numbered 1, 2 and 3 in Fig. 1) is about ten times larger than the model grid size, making it inadequate to consider the river mouth as a single source. To this extent, 10 sensitivity experiments were performed in order to select the appropriate number or location of point sources. The model parameters used are presented in Table 1. In the first six sensitivity runs, each of the three outlets is considered separately using the same discharge rate (i.e., either 1000 or 3000 $m^3\ s^{-1}$). In runs 7 through 10 the three outlets are combined together using either a similar (i.e., runs 7 and 10) or a differentiated discharge rate. Historical anecdotal information of the fluxes in the delta region has indicated that the sources discharge with the proportion of 3:5:2 and such proportion were employed in the simulations.

The plume evolution, as indicated by the successive position of the 34 psu isohaline is presented in Fig. 2. As can be seen, there are clear differences in the horizontal spreading of the single-source plumes under low discharges, which results from the interaction between the brackish water, the local bathymetry, and the shoreline. Spreading of the northern source plume occurs primarily in the northeastward direction, attached to the downstream coast. For the central source plume, it occurs southwards but remaining connected to the upstream coast. Lastly, the southern source plume spreads in the southwestward direction. The

Table 1
Parameters used in the initialization run.

Expt	Source No.	Q_{river} [m^3 s^{-1}]	Depth [m]
1	1	1000	5.28
2	2	1000	7.05
3	3	1000	7.07
4	1	3000	5.28
5	2	3000	7.05
6	3	3000	7.07
7	1 + 2 + 3	3×1000	–
8	1 + 2 + 3	900 + 1500 + 600	–
9	1 + 2 + 3	1800 + 3000 + 1200	–
10	1 + 2 + 3	3×3000	–

Table 2
Wind velocity components (in km/h) including the phases lag (in degrees) used in the experiments with sea-breezes.

Expt	u_0	v_0	u_1	v_1	$\phi_{\tau x}$	$\phi_{\tau y}$
11	0.0	0.0	5.0	5.0	180.0	130.0
12	0.0	0.0	12.0	12.0	180.0	130.0
13	0.0	0.0	18.0	18.0	180.0	130.0
14	−5.67	10.15	7.49	7.15	115.9	−142.9
15	1.41	8.54	5.64	4.75	142.7	−108.3
16	−13.49	0.19	7.21	9.93	103.3	−133.9

horizontal shape of the plume 5 days from initialization is very similar in the case of plumes produced by sources #1 and #2, both under low and high discharge rates. The shape of this early stage plumes comprises a nearly symmetric bulge in relation to source, and a nose of the coastal bulge. Source #3 produces narrower plumes, as they never reach the 50 m (100 m) isobath under low (high) discharges. The maximum alongshore extent attained by the plumes differs considerably in each of the single-source cases, indicating that regardless of the discharge rate, the buoyant flow from the northern source penetrates furthest north, followed by the central source.

Under high discharges, all the plumes spread primarily northeastwards attached to the downstream coast, indicating a dominance of the buoyancy forcing over the effects of topography and shoreline geometry. The shape of these plumes is consistent with the shape of plumes produced in simulations employing a straight coastline (e.g., Garvine, 1999; Fong and Geyer, 2002; Isobe, 2005). Downstream from the river mouth almost all high discharge plumes are projected well offshore, in some cases reaching the 100-meter isobath, precluding the different plume zones from being distinguished at day 45. This projection is not apparent in the shape of any of the single-source plumes, or in the combined sources with a similar discharge of 1000 m^3/s. According to the classification schemes of Chao (1988a) and Kourafalou et al. (1996a), these plumes tend to be diffusive subcritical 30 days after initialization, as illustrated by the comparable widths of the bulge and the coastal current.

The early stage of plumes from multiple sources consists of a bulge with three protuberances that forms soon after the plume is initialized. It then evolves without significant change in shape until day 7, when the brackish water is transported downstream. By comparing the plumes from three sources combined altogether at 3000 m^3/s (Panels 7 or 8) with those from a single source discharging 3000 m^3/s (experiments 4, 5, or 6), three aspects can be pointed out. Firstly, the combined source plume may contain signatures of each individual plume if these are low-discharge plumes. Secondly, the plume from a single source can penetrate further downstream in comparison with the combined-source plume. This pattern is most likely due to the coastline geometry (notice the presence of a headland), and the initial velocity. Lastly, as far as surface salinity is concerned, the limit of influence of each individual plume cannot be distinguished five days from plume generation onwards.

When the combined source plumes are considered with either similar or differentiated discharge rate, the resulting plume shapes differ in two aspects, as illustrated in panels 7 and 8. Differentiated discharge produces plumes with reduced upstream penetration (opposite to the direction of propagation of a Kelvin wave) and increased downstream penetration. Moreover, combined-sources produce a notably more elongated plume because the outflow discharge was increased. This feature suggests that the structure of the Zambezi River plume is influenced by the proportion of freshwater discharge at each source, just as much it is influenced by the delta configuration evidenced in the low discharge experiments (panels 1, 2 and 3).

Although the density-driven flow never reaches the open boundaries in all experiments, a current is generated along the shelf edge (not shown), and as it evolves, on day 26 it becomes strong enough to dramatically induce changes to the near shore flow. This is depicted by the intersection of the isopleths in almost all the experiments presented in Fig. 2, in which some portions of the plume at time $t = 45$ days have retreated in relation to earlier stages. The shelf-edge current is remotely induced by the density driven current through the volume conservation enforcement employed at the domain boundaries to account for the changes in the volume of freshwater. This current showed to be very sensitive to the choice of number and position of the sources, since for example, the freshwater introduced from sources #2 and #3 resulted in a shelf-edge current oriented either toward the southwest or toward the northeast under a discharge rate of 1000 or 3000 m^3 s^{-1}, respectively. These results reveals that the position of the river mouth in relation to the delta (headland) combined with the discharge rate has major implications for the plume spreading. The delta in this case protrudes into the coastal ocean to form a nearly symmetric headland, complicating the near-shore dynamics. It is worth noting that in these experiments, no wind influence is considered for 45 consecutive days. This unrealistic condition is meant only as a qualitative assessment of the influence of the multiple outflows on the near-field plume structure and transport pathways.

2.2.2. Spin-up run and the unforced plume

Using the combined-source with differentiated discharge discussed above (experiment 8) the model was spun-up during 15 days to allow the geostrophic adjustment to occur before submitting the plume to wind action. The spin-up run used a freshwater discharge of 1500 m^3 s^{-1} (i.e., the midpoint of the modal class) and no wind forcing. The unforced plume is obtained by running the model for another 7 days (i.e., the length of integration). The horizontal distribution of salinity and velocity of at the end of spin-up run and the unforced plume is presented in Fig. 3. The unique difference is the dimension of the alongshore and across-shore plume extents. The vertical structure of the unforced plume at day 22 is presented in Fig. 4, where salinity and velocity profiles are plotted against the distance from the coast in kilometers. As can be seen, in all transects, the bottom layer contains only ambient water, and the plume waters are limited to a thin layer at the surface, whose thickness varies between 2 and 4 meters at the coast. Near the river sources, the bottom layer moves landwards (panels B and C), opposing the flow of freshwater in the upper layer. The coastal current has a relatively intense flow (∼10 cm/s), and weak vertical gradient of salinity compared with the rest of the plume.

In summary, in the absence of additional external forces, a moderate and constant freshwater discharge generates a surface-advected plume, in contrast with the bottom-advected plume found when a flat topography is employed (Nehama and Reason, 2015). After 22 days, the plume spreads over the area defined by the latitudes 18°S–19.1°S and the 50-meter isobath. The maximum plume thickness is smaller than 5 meters in the entire plume extension, and a shoreward oriented undercurrent exists in the periphery of the sources.

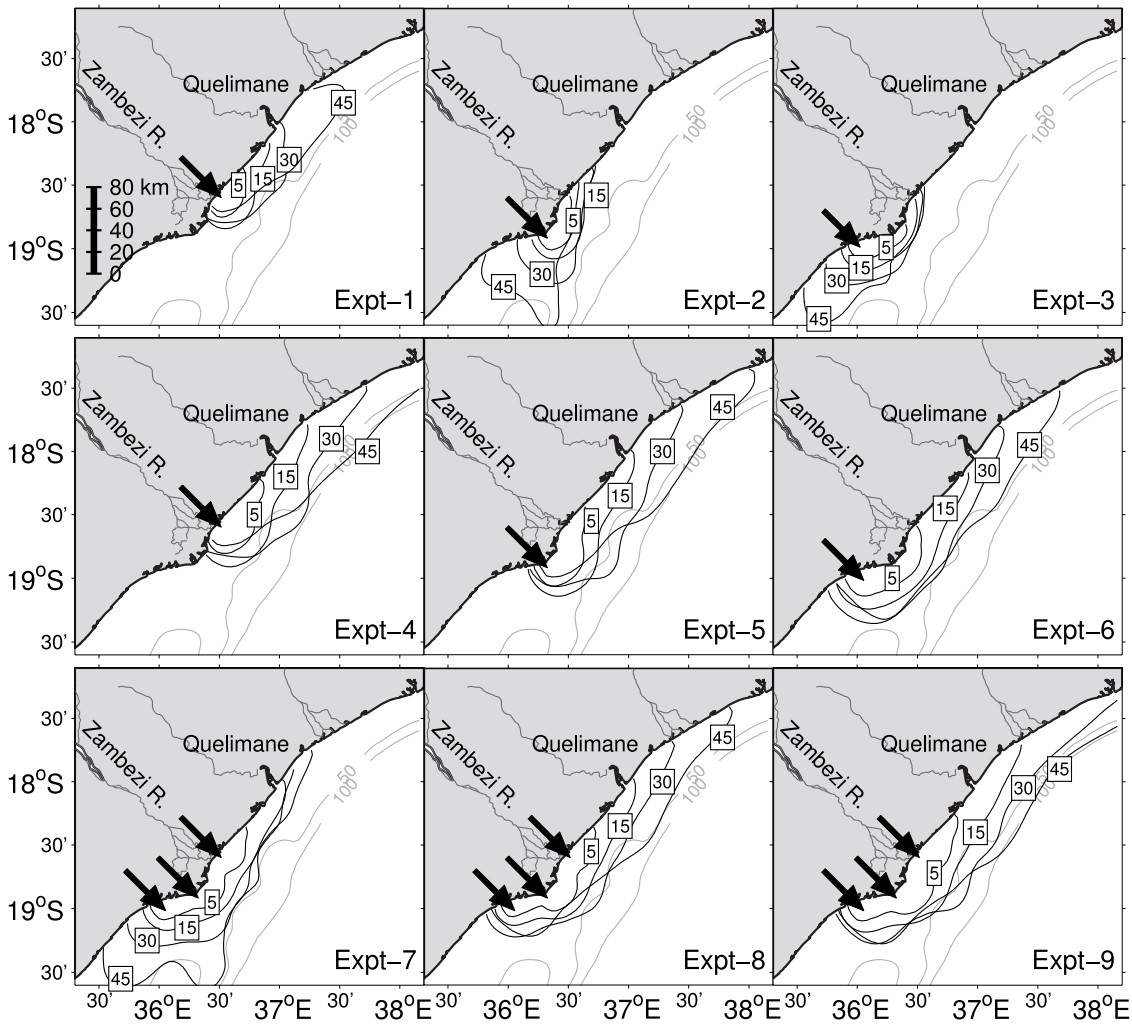

Fig. 2. Location of isohaline of 34 psu at day 5, 15, 30 and 45 for different conditions of buoyancy input, here characterized by the number and location of point sources, as well as the total discharge. Parameters used in the different experiments are presented in Table 1. The dark arrows over land indicate the quantity and relative position of point sources. The gray contours correspond to the 50 and 100 m isobaths, here plotted for reference.

3. Plume forced by impulsive winds

The structure of freshwater plumes under the action of an impulsive wind field is considered below. Apart from the river discharge, the dynamics of the coastal waters were forced by wind stress under the influence of the Coriolis Effect. In order to assess the plume response to wind forcing, two sets of numerical experiments were considered, one using a constant wind stress and another using a 24-hour period oscillating wind stress, both having a uniform distribution over the entire model domain. In these experiments, the winds blew over a pre-existing plume (i.e., wind stress turned on from the end of spin-up, on day 15). In the experiment with constant winds, the kinematic surface flux of momentum was expressed in terms of the quadratic friction law, as follow,

$$(\tau_x, \tau_y) = \rho_{air} C_d \left(\sqrt{u_s^2 + v_s^2}\right) \cdot (u_s, v_s) \tag{1}$$

Where τ_x and τ_y are the components of wind stress, ρ_{air} is the air density here taken as $\rho_{\text{air}} = 1.2$ kg m^{-3}. u_s and v_s are the wind velocity components at the surface level, and C_d is the drag coefficient here taken as constant and $C_d = 0.0013$.

For the second experiment, our parameterization of the periodic winds (or sea-breezes) followed the analysis of Hyder et al. (2002), who suggested that the wind stress can be represented by the sum of two components, i.e., a daily mean, τ_0, and an oscillating part having amplitude τ_1, and phase difference ϕ_τ, as follows,

$$\begin{cases} \tau_x = \tau_{0x} + \tau_{1x} \cos(\omega t + \phi_{\tau_x}) \\ \tau_y = \tau_{0y} + \tau_{1y} \cos(\omega t + \phi_{\tau_y}) \end{cases} \tag{2}$$

The daily mean stress components τ_{0x} and τ_{0y} can be calculated by averaging low frequency wind data over a relatively long period, and the amplitude and phase of the sea-breeze component can be derived from a regression analysis of high frequency wind data. The periodic components in Eq. (2) result in a vector whose orientation throughout the 24-h cycle describes an ellipse, and therefore, it is possible to choose the ellipse phases ($\phi_{\tau x}$ and $\phi_{\tau y}$) so that the orientation of the major axis matches the observed predominant wind direction.

3.1. Response to constant winds

Following the spin-up, a constant wind stress was turned on and sustained for 7 days. Two wind magnitudes (5 and 12 km/h) representing weak and moderate conditions were tested, along with eight wind directions characterizing the four major directions (i.e., north, west, south, east), and a clockwise rotation by 40° from the model coordinate system. This rotation resulted in a

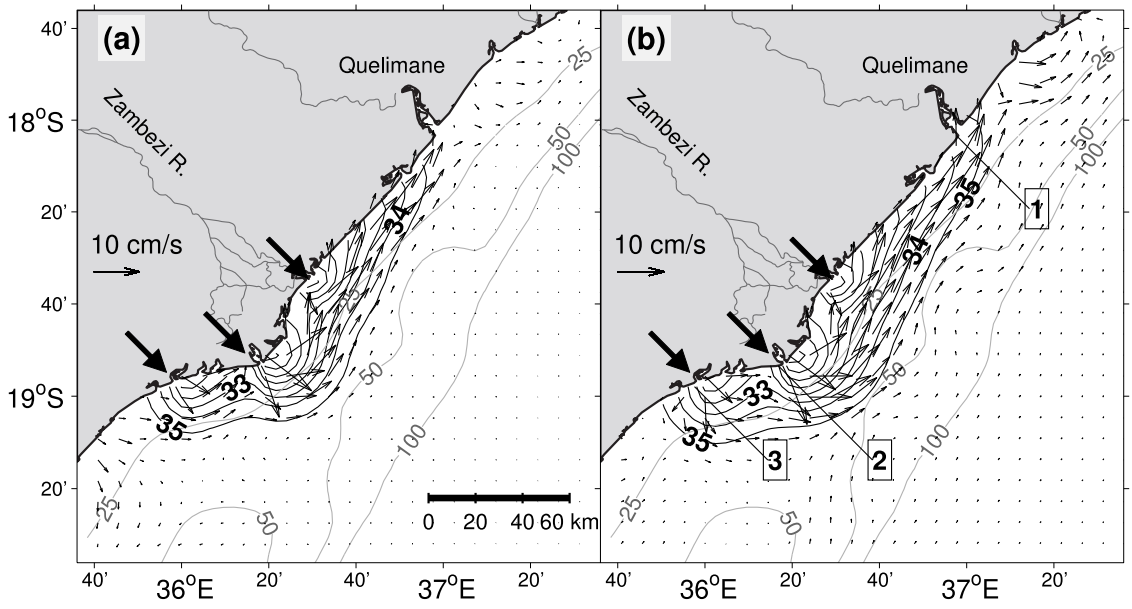

Fig. 3. Horizontal distribution of surface salinity (contours) and velocity field (arrows) simulated for a discharge of 1500 m^3 s^{-1}. (A) Initial conditions for the experiments with external forcing, $t = 15$ days. (B) Unforced plume at $t = 22$ days. Velocity vectors are plotted every other gridpoint, and contours are 28 to 35 by 1 psu.

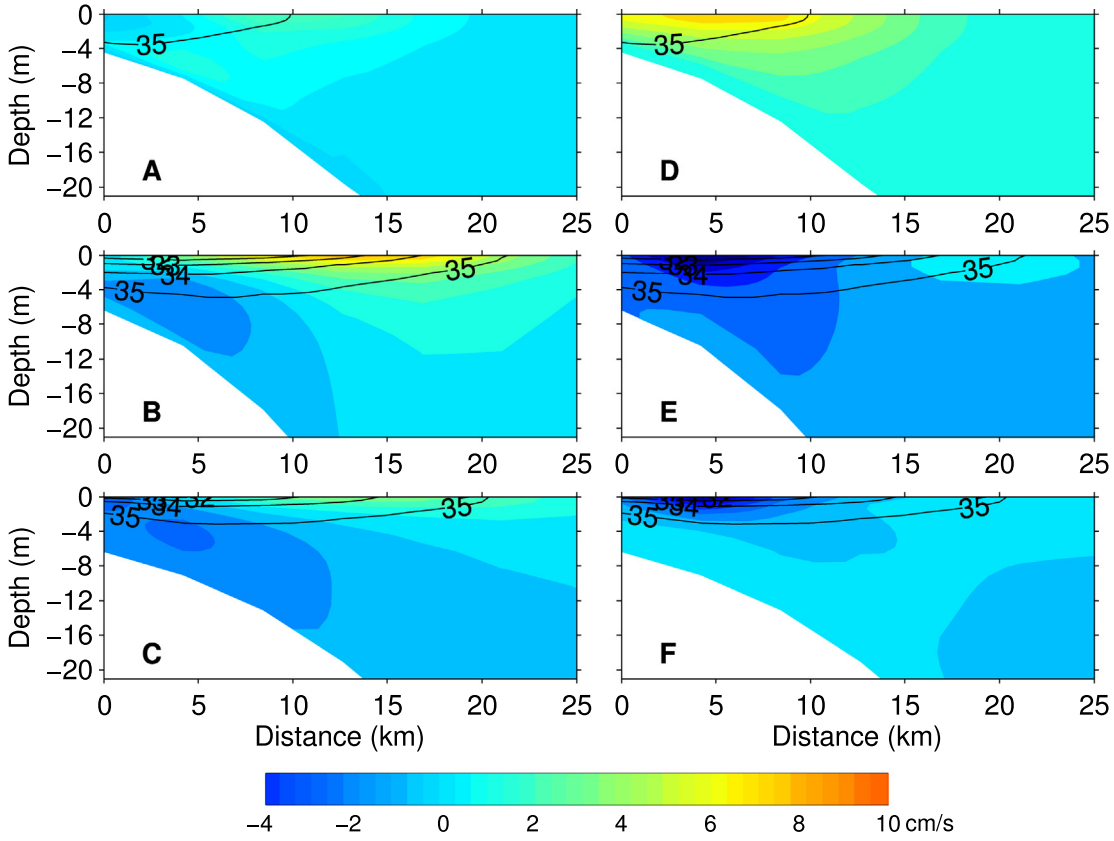

Fig. 4. Vertical distribution of the cross-shelf (left) and along-shelf (right) velocity components overlaid by salinity contours (C.I. is 1 psu) computed for the model time $t = 22$ days. From top to bottom, transect 1, 2, and 3 illustrated in Fig. 3b.

local "alongshore"-"across-shore" coordinate system (Kourafalou et al., 1996b). It is worth mentioning that tests with stronger wind conditions often resulted in model crash due to numerical instabilities, and for that reason, the response to strong winds are not discussed here.

Under the action of weak or moderate winds, the buoyant discharge was spread downwind in all the 16 cases analyzed, resulting in a plume shape that can be categorized in two groups, namely, ones exhibiting a "large bulge", and those featuring a "coastal current". These groups were identified according to the

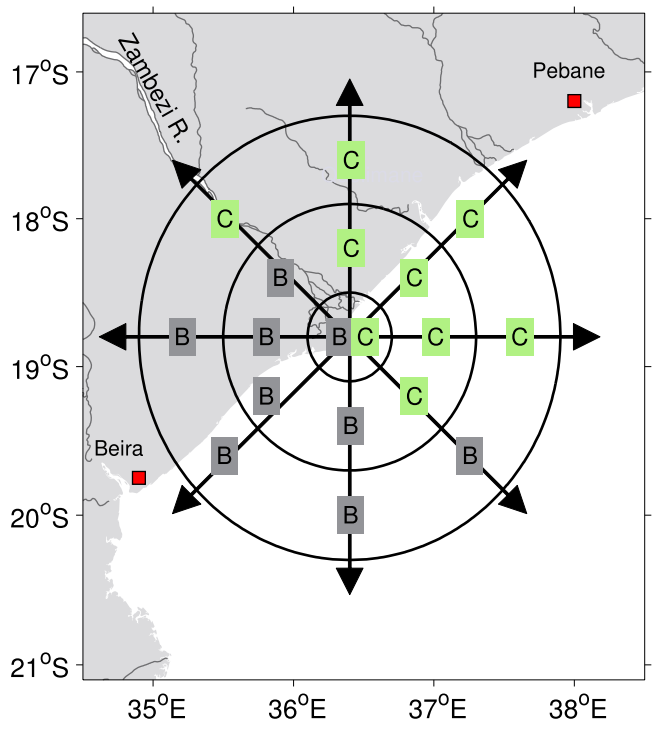

Fig. 5. Shape of plume classified as bulge (B) or coastal current (C), as simulated for a discharge of 1500 $m^3\ s^{-1}$ under different wind conditions. The inner circle represents the spin-up results (no wind forcing), the middle circle represents the weak winds (5 km/h), and the outer circle represents the moderate wind conditions (12 km/h). The arrows indicate the wind direction.

horizontal distribution of surface salinity combined with the direction of the flow attained at the end of the 7-day period of wind forcing. Examples are presented in Fig. 6, with the large bulge group presented in the four panels on the right-hand side. The downwind transport of plume waters is in good agreement with earlier studies on buoyant discharges over shallow and sloping topography (Chao, 1988a; Kourafalou et al., 1996b), as well as the theory of Ekman transport (Kampf, 2009; Cushman-Roisin and Beckers, 2009). None of the plumes featuring a coastal current extended as far north as the mouth of the Licungo River located about 180 km from the Zambezi Delta, with the exception of plumes forced by westerly and southwesterly winds. Additionally, none of the plumes featuring a large bulge near the sources extended offshore beyond the 100-meter isobath, except for those forced by moderate northerly and northeasterly winds. The "large bulges" were formed under northerly, northeasterly, easterly, and northwesterly wind cases (Fig. 5). Winds blowing in these directions induce a surface current near the freshwater sources that is oriented either seawards, or along the coast toward the southern model boundary. These surface flows inhibit the development of a buoyant flow in the downstream direction, and promote the accumulation of freshwater immediately in front of the delta. Depending on the magnitude of wind stress, the shape of the bulge changes from symmetric in relation to source #2, to distorted (i.e., displaced toward the south or north).

Plumes that feature a "coastal current" were produced under westerly, southerly, southwesterly, and southeasterly winds (Fig. 5). The largest downstream penetration of the coastal current was found under the action of weak positive alongshore and moderate southerly winds, and it reached about 140 km downstream, measured from the source #1. However, the maximum penetration distance in the remaining cases that resulted in a coastal current was not very different from this value, as the shortest penetration was about 110 km. On the other hand, the upstream penetration varied considerably from almost zero to a few kilometers measured from source #3. The upstream penetration did not depend much on the intensity of wind stress but rather on the strength of the wind-driven ambient current generated upstream from the plume (around 19.5°S). The width of the bulge was in the range of 0.5–1.5 times greater than the width of the coastal current estimated halfway to the nose of the current. Meaning that in some cases, the bulge and coastal current could not be distinguished. According to the classification schemes of Chao (1988b) and Kourafalou et al. (1996b), these plumes are classified as subcritical to diffusive-subcritical.

These plume responses to wind forcing are summarized in association with the alongshore component of the wind, as follows. While "large bulge" plumes are produced under upwelling favorable winds, a downwelling favorable wind produces a "coastal current" plume type, in agreement with previous observational (Lentz and Largier, 2006) and analytical (Moffat and Lentz, 2012) considerations of the plume response to wind forcing.

This result is particularly interesting because the easterly winds (upwelling favorable) and the southeasterly winds (downwelling favorable) are amongst the dominant wind fields in the region surrounding the Zambezi Delta, suggesting that the synoptic plume structure will be very sensitive to the magnitude and duration of wind events. In fact, by order of frequency, the most dominant winds are southerlies, southeasterlies, easterlies, and northeasterlies. The specific changes to the nearshore flow induced by these wind fields are presented below, following the discussion of Chao (1988a). The resulting primary orientation of plume spreading does not always coincide with the predominant orientation of the surface flow, as indicated by the velocity vectors in panels B and F in Fig. 6. In these specific cases, the part of the surface flow directed southwestwards, which favors the existence of a large bulge, is as strong as the part of the flow directed northeastwards, which favors the existence of a coastal current.

Southerly winds, as well as the southwesterly (downwelling favorable) winds, induce a motion of plume waters oriented primarily northeastwards along the coast, similar to the orientation of the flow in the unforced plume case. Near the coast, the movement of surface water is constrained by the landmass; hence during weak winds they cause the whole circulation to be oriented downwind. The circulation is weak everywhere, except in the plume region downstream from the river mouth where the wind-induced and the buoyancy-driven flows interact and ultimately form a strong coastal jet along the coast (characterized by an intense two-layer flow of plume waters flanked by relatively slower flow of ambient waters). Under the action of moderate winds, the coastal jet is replaced by a wind-driven coastal current, whose width increases toward the plume's leading nose. The moderate winds inhibit the upstream penetration of plume waters, as well as the across-shelf motion, resulting in massive deepening of the plume near its sources. Hence, plumes that are forced by moderate winds remain connected with the seabed near the coast, and are classified as bottom-advected plumes.

Southeasterly winds induce movement of plume waters toward both the southwest and the northeast direction. The movement of surface waters near the coast is directed shoreward, which inhibits the seaward export of plume waters. Apparently, the interaction between the model geometry (presence of a headland) and the shoreward flowing surface water results in flow separation offshore from the headland.

Plume waters then flow along the coast and away from the sources in both directions (downstream and upstream). There is also a possibility that coastal set-up also contributes to the flow separation in front of the headland. Either way, the part of the

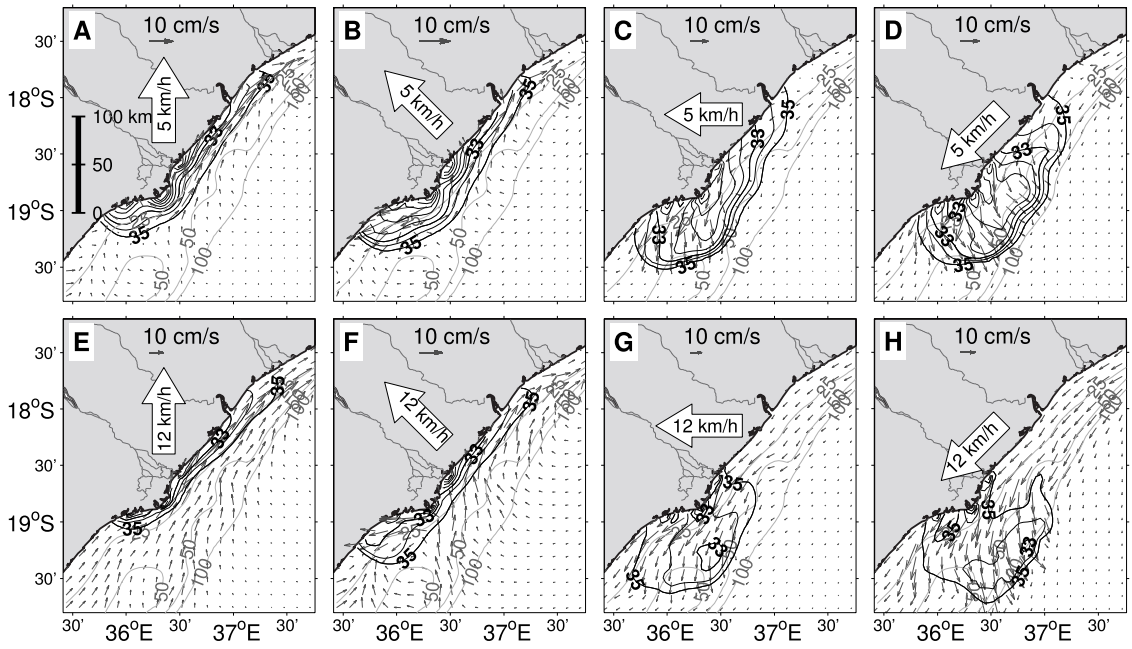

Fig. 6. Horizontal distribution of surface salinity (contours) and velocity field (arrows) simulated for a discharge of 1500 m^3 s^{-1} at the time $t = 22$ days. Velocity vectors are plotted every other gridpoint, and contours are 28 to 35 by 1 psu. The large arrow over land and its inscription indicate the wind direction and magnitude, respectively.

plume flowing upstream becomes wider than its downstream counterpart is, by virtue of geostrophic forces.

Easterly winds drive the movement of near-shore water toward the southwest, i.e., opposing the direction of a Kelvin wave. Hence, within the reach of plume waters, stratification weakens the wind-driven flow and the freshwater is projected offshore, by virtue of the Coriolis force.

Northeasterly (upwelling-favorable) winds also termed negative alongshore winds, produce a plume response similar to the easterly winds (panels C and D in Fig. 6), except for the greater seaward intrusion of plume waters, as well as the enhanced horizontal mixing between the plume and ambient waters. Since the plume does not feel the bottom, it was transported seaward by the wind as if there was no friction between plume and ambient waters, and apparently, the plume had no influence from the landmass or coastline.

3.2. Daily oscillating winds

Coastal systems are often subjected to the action of breezes in which the wind direction and intensity change during the day, with its vector following an elliptical trajectory. In order to investigate the influence of this wind field on a pre-existing plume, an experiment was conducted consisting of two sets of model runs, using a constant discharge of Qriver=1500 m^3/s and the idealized sea-breezes described in Eq. (2). This discharge corresponds to the midpoint of the modal class, or simply the realistic mean value observed during the dry-season. For sea breezes, the phase difference, ϕ_τ, and the wind velocity components used to compute the mean magnitude, τ_0, and the sea-breeze amplitude, τ_1, were varied as indicated in Table 2.

The breeze was imposed from the end of the spin-up run and sustained for 7 days. The first set of model runs (experiments 11, 12, and 13 in Table 2) aimed at investigating the plume response to symmetric sea breezes having their major axis oriented landwards and magnitude chosen to vary between 5, 12, and 18 km/h, corresponding to the Beaufort numbers 2 through 4 (light, gentle, and moderate breezes). The orientation of ellipsoids in these experiments is in good agreement with observed average direction of QuikSCAT winds (Nehama, 2012).

The second set of model runs explored plume response to asymmetric breezes. The sign of the averaged wind velocity components (u_0 and v_0 in Table 2) determines the quadrant in which the center of the ellipsoid is located, and hence, the orientation of the wind forcing, while the phase difference between the x- and y-component determines the ellipse's orientation. The orientation in experiments 14 to 16 varied between 237° and 259°, corresponding to 10 km/h landward (or southeasterly) breezes, 7 km/h southwesterly breezes, and 12 km/h easterly breezes. The asymmetric breezes were extracted from the high frequency outputs of a weather prediction model (WRF) configured for the study region (Maúre, 2013).

The top panels of Fig. 7 present the horizontal distribution of salinity and velocity averaged over 1 cycle of symmetric sea breezes, 7 days after the winds were switched (panels B, C, and D representing experiments 11, 12, and 13). The unforced plume at time $t = 15$ days is also shown for reference in panel A. By comparing the downstream position of the 35 psu isohaline in these four panels, which is an indication of the maximum alongshore plume extent, it can be seen that the plume penetrates about 25 km further downstream when forced by symmetric sea breezes. However, no noticeable difference exists in the seaward penetration of the plume, except for the spacing of salinity contours that is considerably larger under sea breezes. In fact, the contours are displaced landwards as the sea breeze intensifies, suggesting an enhancement of the horizontal and vertical mixing associated with the periodic wind forcing. The horizontal velocity field within the plume changes significantly from the "no-wind" to the case of 18 km/h breezes. The magnitudes of the time-averaged surface flow are very similar in the cases of "no-wind" and a sea breeze of 5 km/h, suggesting that light breezes have only a minor effect on plume structure. While the speed at surface is lower for plumes forced by 12 and 18 km/h breezes (i.e., gentle and moderate breezes), in comparison with the "no wind" case.

Unlike the time-averaged flow, the transient flow (ellipsoids not shown) indicates that the amplitude of the surface flow

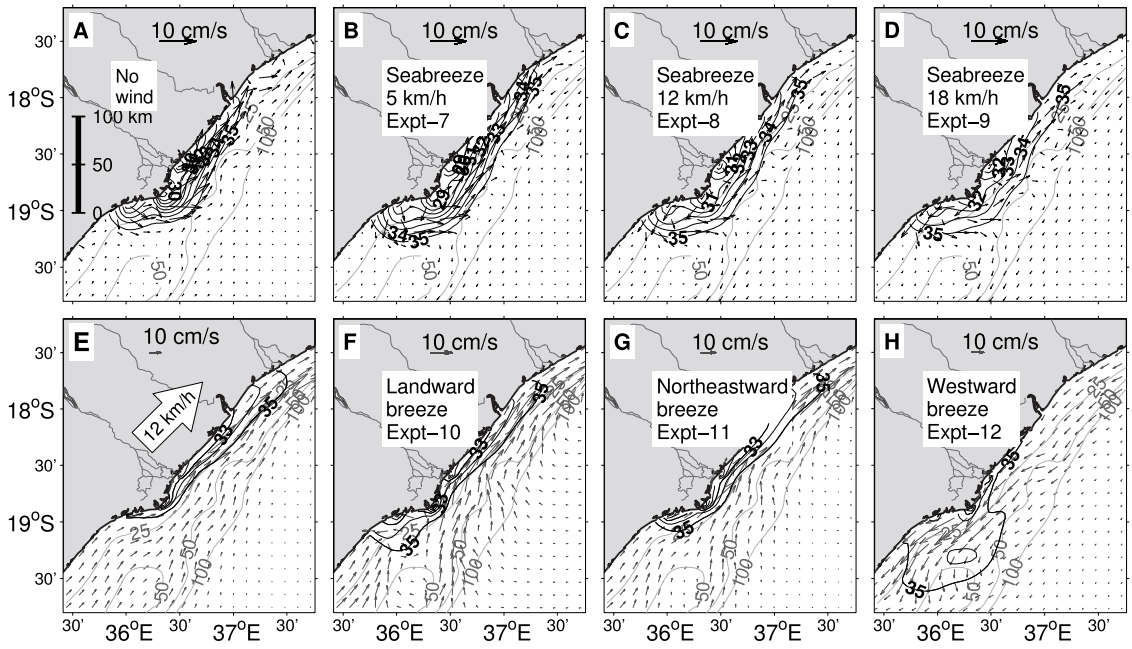

Fig. 7. Horizontal view of surface salinity (contours) and velocity (arrows) fields averaged over one cycle, for the following wind conditions: (A) no wind forcing; (B through D) after 7 days of symmetric sea breezes started from (A), with maximum wind intensity indicated by text in each panel.

increases considerably with the sea-breeze intensity. In all cases, the trajectories in the offshore region are predominantly circular, changing to elliptic near the coast. The orientation of the semi-major axis of the ellipses along the coast changes from northward in the case of a 5 km/h breeze magnitude, to northeastward in the remaining cases, while the eccentricity decreases with the intensity of sea breezes. In addition, the surface flow in the plume region is not in phase with either the flow in the offshore region, or the wind forcing. The zonal component of the near-shore velocity is ahead of the wind by nearly 7 h, while the meridional component is lagged by 2 h.

The effect of asymmetric sea breeze forcing on a pre-existing plume is displayed in the bottom panels of Fig. 7, along with the plume forced by a moderate constant southwesterly wind (Panel 7E). The constant wind have similar orientation as the synoptic component of sea-breezes used in panel 7G. The plumes in panels F and H have their synoptic component aligned along the landward (i.e., northwestward) and westward direction, and the corresponding constant wind plume is presented in panels F and G of Fig. 6. A comparison of the plume shapes produced by constant winds and an asymmetric breeze reveals that the magnitude and orientation of the permanent component of sea-breeze dictate the pattern of plume spreading. In each case addressed in experiments 14 to 16, the seaward as well as the along-shelf plume extents is either reduced or similar to that produced under constant wind forcing, indicating that no additional lateral penetration of the plume is promoted by the periodic winds.

Fig. 8 displays the vertical distribution of salinity and mixing coefficient expressed in terms of vertical eddy viscosity. As can be seen, a weak symmetric breeze produces a plume with similar structure to the unforced plumes, characterized by a surface-advected plume confined in the upper 5 to 7 meters and off-shore penetration reaching beyond 25 km from the coast. The plumes produced under constant winds and asymmetric breezes have notably shorter offshore penetration and deeper vertical entrainment.

4. Discussion

Very often, numerical simulations of unforced buoyant discharges over constant slope topography present a bulge of re-circulating flow that is strongly affected by river inertia and Earth's rotation. In this study, the structure of a freshwater plume was investigated through a series of numerical simulations that aimed at identifying the role played by wind forcing on the plume's horizontal and vertical structures. Realistic geometry and bathymetry were adopted, as a first step toward a realistic simulation of the Zambezi River plume.

One of the main features of the Zambezi River is the deltaic form of its mouth, and most importantly, the fact that the delta constitutes a sizable headland with potential impacts on the near-shore circulation. The simulations presented here suggest that under low discharges, each of the three main mouths produces a plume with dispersion patterns that differ greatly from the other two, because of the dissimilar distribution of surface pressure at the coast. By the fifth day of computation, the plumes from the northern and central sources spread radially, while the southern river mouth generates a plume bent northeastwards. This curved shape of the plume from the southernmost mouth is somewhat consistent with observations of the Elwha River plume along the Strait of Juan de Fuca (Olympic Peninsula, Washington) reported by Warrick and Stevens (2011). The difference being that the bending is not induced by the ambient flow as it happens in the Elwha plume, but instead by the buoyancy-driven flow from the southernmost mouth of the Zambezi River. Under moderate and high discharges, no significant difference in the spreading of the plumes is evident, except the fact that the coastal current produced under combined sources is wider and penetrates further downstream. In the absence of external factors, such as winds, tides, and ambient currents, a modest discharge of freshwater forms an estuary plume trapped to the coast that propagates northeastwards along the coast, in agreement with the downstream propagating plumes widely reported in the literature (Chao, 1988a; Oey and Mellor, 1993; Garvine, 1999; Jurisa and Chant, 2013; Nehama and Reason, 2015). No clear distinction between the bulge and coastal current regimes were found, which

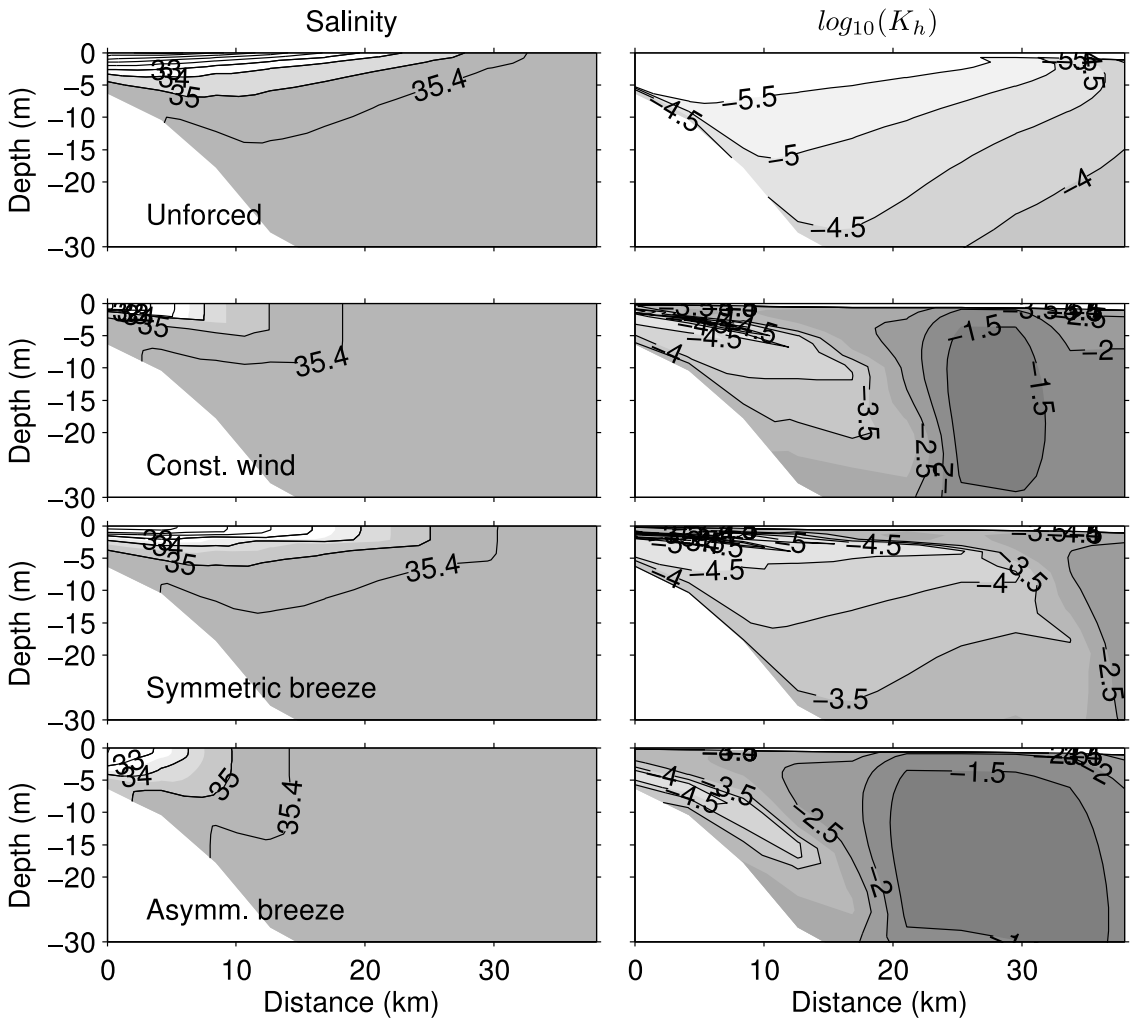

Fig. 8. Vertical distribution of salinity, and mixing coefficient (K_V in m^2s^{-1}) along the cross-shelf transect number 2 displayed in Fig. 3. Data simulated for four different wind forcing, namely, no wind stress, a constant moderate wind (southeasterlies of 12 km/h), a symmetric sea-breeze (12 km/h of intensity), and an asymmetric breeze with a permanent component that is similar to the constant wind. The data is presented for the model time, $t = 50$ days in the case of unforced plume, and at 7 days from the beginning of the wind forcing for the wind forced cases.

is a typical result for numerical simulations employing realistic geometry and bathymetry (Pimenta et al., 2005; Kourafalou et al., 1996b), and re-circulation in front of the river mouth was not apparent. However, due to the initially radial dispersion, portions of freshwater were found moving southwards (upstream) to a point where they turn anticlockwise and flow toward the downstream coast. This reversal of the flow could be associated with an offshore projection of coastal water as it passes through source #3. The circulation patterns of this unforced plume and the length scale associated with this upstream portion of freshwater do not seem enough to explain the upstream flow of brackish water beyond 20°S found in the observations presented by Nehama and Reason (2014). The discrepancy is related to the fact that an idealized forcing was used in this simulation, not to mention the influence that the choice of the imposed outflow orientation, absence of tides and ambient shelf circulation might have on the results.

It was found that regardless of the initial stratification set by the choice of bathymetry dataset, the wind-forced simulations produce two distinct patterns of plume dispersion, which due to their shapes were termed "large bulge" and "coastal current". The large bulges are characterized by a large portion of freshwater flowing offshore to about 65 km from the coast, between the coastline and the 100-meter isobath. This offshore extent of the plume is within the limits observed in earlier studies (Lutjeharms, 2006; Nehama and Reason, 2014). The surface flow within the plume waters varied from seaward to southwestward depending on the orientation and intensity of the wind stress. On the other hand, plumes that resulted in a coastal current displayed a maximum downstream penetration that varied according to the orientation and magnitude of the wind stress. These parameters also influenced the ratio of plume width at the source to the width of the coastal current halfway to the nose. These plumes correspond to the surface-advected plumes of Moffat and Lentz (2012) that have a large portion of their total width detached from the bottom, and their structures experience massive changes with the onset of winds, including the above mentioned along-shelf (downstream) transport.

In general, the winds acting on the surface layer dictated the movement of the plume and ambient waters. Between the shoreline and the 100-meter isobath, all flow was constrained by the presence of landmass, resulting in along-shelf flow oriented either northeastwards or southwestwards, and a more intense cross-shelf flow. The plume waters in particular, were transported to the left of this modified wind-induced surface flow, whose orientation at the surface varied between >15° and 90° in the case of large bulges, and between 0° and 180° in the case of coastal current. Due to the intensified cross-shelf flow, the coastal

currents became narrower as the wind intensity increased, while the large bulges became wider under stronger winds. The plume response to constant winds was examined before by Kourafalou et al. (1996b) and Chao (1988b), and the dispersion patterns presented here agree with these previous studies.

The wind conditions that resulted in a large bulge comprise both weak and moderate winds whose alongshore component is negative, as well as seaward winds. It is worth noting that the large bulge constitutes a plume shape that resembles fairly well the ship-based in-situ observations reported by Nehama and Reason (2014), in contrast with the shapes produced when no other external forcing is applied in the simulation.

Our model simulations reproduced reasonably well the observed upstream transport of plume waters, reaching nearly 100 km from the mouth in some cases, but they failed to produce a concurrent downstream transport of freshwater in a coastal current significantly narrower than the upstream counterpart is. We speculated that, in contrast to the portion of brackish water moving downstream, the upstream transport is a process purely driven by the winds, and most likely, it is influenced by the imposed east–west orientation of the outflow. Based on results from numerical simulation and references to observational evidence, Kourafalou et al. (1996b) pointed out that a downstream buoyancy-driven current near the coast can very likely coexist with an upstream wind-driven flow during periods of strong river discharges and light upwelling-favorable winds.

The plume response to oscillating winds was studied through a number of simulations that included a uniform and symmetric sea-breeze forcing of varying magnitude oriented predominantly landward, as well as an asymmetric sea-breeze with varying orientation, both blowing over a pre-existing plume fed by a constant discharge of 1500 $m^3\ s^{-1}$. The resulting plume response to the diurnal oscillation of winds can be summarized as follows.

The daily and uniform symmetric breezes seem to be ineffective in driving a daily variability of the plume, since every effort to move away brackish waters is, 12 h later, compensated by a similar effort to bring the plume to its initial position. In other words, the integral of shear stress exerted by the wind field in 24 h reduces to zero. The plume response to this forcing can however be noticed in the sub-daily scale. For instance, the Hudson River plume is also constantly under the influence of land-sea breezes. There are reports indicating that when the breezes attain a near-zero mean speed, the Hudson plume responds to forcing by increasing the accumulation of freshwater in the bulge, and also doubling the speed of the nearshore currents (Chant et al., 2008; Hunter et al., 2007, 2010). However, in most real systems the breezes are hardly symmetric or maintain the near-zero mean speed for long periods because the land/sea temperatures and hence atmospheric pressure fields vary significantly during the 24-hr period, and the plume will rather respond to the asymmetric forcing.

Asymmetric breezes (i.e. consisting of a synoptic and a diurnal component) induce motions of plume waters in the same fashion as a constant wind having the same magnitude and orientation of the non-zero synoptic component of the wind. The only difference between the responses is the enhanced vertical mixing under asymmetric breezes, in relation to the constant wind, which results from the shear instability between the plume and the underlying ambient waters (Stumpf et al., 1993; Pinones et al., 2005). The simulation-based responses described above are supported by the in situ observations of Pinones et al. (2005), who found that the Maipo River plume propagates upstream off the central coast of Chile during periods of intense sea-breeze activity (predominantly oriented landwards). Despite the small scale of the variability noticed throughout the day, the difference between daytime and nighttime wind stress (i.e., spinning up and relaxing regimes) ultimately drives the synoptic dispersion of the plumes.

The simulation forced by freshwater discharge of 1500 $m^3\ s^{-1}$ and asymmetric easterly breezes resulted in a horizontal distribution of salinity much closer to observations, and it consisted of a massive bulge of brackish water propagating upstream, and a portion of water in a narrow segment downstream from the river mouth. The plume exhibited a surface-advected structure, in agreement with the earlier observations (Nehama and Reason, 2014).

5. Summary

In the absence of external factors such as winds, tides, and ambient currents, a modest discharge of freshwater from the Zambezi River forms an estuarine plume in the Sofala Bank, which then propagates northeastwards trapped to the coast. The response of a pre-existing buoyant plume to intensive wind forcing is marked by either a change in the energy available for mixing, or by a movement of surface waters to left of the wind direction. It was found that for a constant wind field, the most striking feature is this wind-induced movement is the Ekman drift of low salinity buoyant waters. When combined with the local geometry and bathymetry, the Ekman drift results in either plume motion offshore to the location of the 100-meter isobath, or downstream attached to the coast to approximately 17.5°S, or even upstream as far as 20°S. The occurrence of upstream and seaward penetration of plume waters is associated with winds having a negative alongshore component (e.g., northeasterly), and/or winds that resulted in seaward or southwestward movement of surface water. During wind conditions favorable to a downstream coastal current, the upstream counterpart of the transport is nearly insignificant, with extents varying from zero to few kilometers. In contrast, wind conditions favorable to the upstream transport often allowed the presence of significant amount of plume waters in the downstream region, despite the southwestward orientation of the velocity vectors.

Symmetric sea breezes have shown to be ineffective in advecting plume waters to large distances. This conclusion comes from the similarities found between the shape of the unforced plumes and those forced by symmetric breezes of different intensities. Hence, response of the plume to these breezes was marked primarily by the enhancement of vertical and horizontal mixing, which translates to a depth invariant structure and a reduced seaward spreading of plume. The asymmetric sea breezes have non-zero magnitude when averaged over the 24-hour cycle, and for this reason, the response of the plume to this type of wind forcing comprises a combination of the responses for constant winds and symmetric breezes. Given that these breezes most likely represent the actual wind conditions, the overall plume dispersion pattern may be strongly determined by the permanent component of the wind field, while the transient features as well as the vertical structure of the plume will be governed by the magnitude and orientation of the oscillatory part of the wind field. The analysis of the response to realistic sea-breeze forcing, with intensity maintained constant for over 7 days, indicated that the plume waters are transported nearly 120 km downstream, 75 km upstream, and 65 km seaward.

CRediT authorship contribution statement

Fialho P.J. Nehama: Conceptualization, Methodology, Software, validation, Formal analysis, Investigation, Writing, Visualization. **Chris J.C. Reason:** Conceptualization, Resources, Supervision, Funding acquisition.

Declaration of competing interest

The authors declare that they have no known competing financial interests or personal relationships that could have appeared to influence the work reported in this paper.

Acknowledgments

This study was funded by the Science Initiative Group at the Institute for Advanced Studies, USA through the (WIO) RISE program and the International Foundation for Science, Sweden through grant contract number w5384-1.

References

Avicola, G., Huq, P., 2003. The characteristics of the recirculating bulge region in coastal buoyant outflows. J. Mar. Res. 61, 435–463.

Backeberg, B., Reason, C.J.C., 2010. A connection between the south equatorial current north of madagascar and mozambique channel eddies. Geophys. Res. Lett. 37 (L04), 604. http://dx.doi.org/10.1029/2009GL041950.

Banas, N.S., MacCready, P., Hickey, B.M., 2009. The 667 columbia river plume as cross-shelf exporter and along-coast barrier. Cont. Shelf Res. 29, 292–301.

Beilfuss, R., dos Santos, D., 2001. Patterns of Hydrological Change in the Zambezi Delta, Mozambique. Tech. rep. Program for the Sustainable management of Cahora Bassa dam and the lower Zambezi valley, working Paper #2.

CFM, 2008. Information and Regulation Guide. Beira Oil Terminal, Beira.

Chant, R.J., Glenn, S.M., Hunter, E., Kohut, J., Chen, R.F., Houghton, R., Bosch, J., Schofield, O., 2008. Bulge formation of a buoyant river outflow. J. Geophys. Res. 113 (C01), 017.

Chao, S.-Y., 1988a. River-forced estuarine plume. J. Phys. Oceanogr. 18, 72–88. http://dx.doi.org/10.1175/1520-0485(1988)018{\T1\textexclamdown}0072:RFEP{\T1\textquestiondown}2.0.CO;2.

Chao, S.-Y., 1988b. Wind-driven motion of estuarine plumes. J. Phys. Oceanogr. 18 (8), 1144–1166. http://dx.doi.org/10.1175/1520-0485(1988)018{\T1\textexclamdown}1144:WDMOEP{\T1\textquestiondown}2.0.CO;2.

Collins, C., Reason, C.J.C., Hermes, J.C., 2012. Scatterometer and reanalysis wind products over the western tropical Indian ocean. J. Geophys. Res. 117 (C03), 045. http://dx.doi.org/10.1029/2011JC007531.

Cushman-Roisin, B., Beckers, J.-M., 2009. Introduction To Geophysical Fluid Dynamics: Physical and Numerical Aspects. Academic Press.

Durski, S.M., Glenn, S.M., Haidvogel, D.B., 2004. Vertical mixing schemes in the coastal ocean: Comparison of the level 2.5 Mellor-Yamada scheme with an enhanced version of the K profile parameterization. J. Geophys. Res. 109 (C01), 015. http://dx.doi.org/10.1029/6902002JC001702.

Fong, D.A., Geyer, W.R., 2002. The alongshore transport of freshwater in a surface trapped river plume. J. Phys. Oceanogr. 32, 957–972. http://dx.doi.org/10.1175/1520-0485(2002)032{\T1\textexclamdown}0957:TATOFI{\T1\textquestiondown}2.0.CO;2.

Gammelsrød, T., 1992. Variation in shrimp abundance on the sofala bank, mozambique, and its relation to the Zambezi River Runoff, Estuarine. Coast. Shelf Sci. 35, 91–103. http://dx.doi.org/10.1016/S0272-7714(05)80058-7.

Garvine, R.W., 1999. Penetration of buoyant coastal discharge onto the continental shelf: A numerical model experiment. J. Phys. Oceanogr. 29, 1892–1909. http://dx.doi.org/10.1175/1520-0485(1999)029{\T1\textexclamdown}1892:POBCDO{\T1\textquestiondown}2.0.CO;2.

Garvine, R.W., 2001. The impact of model configuration in studies of buoyant coastal discharge. J. Mar. Res. 59, 193–225, artifacts in buoyant coastal discharge models: An observational and model study.

Hetland, R.D., 2005. Relating river plume structure to vertical mixing. J. Phys. Oceanogr. 35, 1667–1688. http://dx.doi.org/10.1175/JPO2774.1.

Hoguane, A.M., 1997. Shrimp abundance and river runoff in Sofala Bank - The rule of Zambezi. In: Workshop on sustainable use of the Cahora Bassa Dam, pp. 16.

Hunter, E., Chant, R., Bowers, L., Carter, G.S., Kohut, J., 2007. Spatial and temporal variability of diurnal wind forcing in the coastal ocean. Geophys. Res. Lett. 34 (L03), 607.

Hunter, E., Chant, R.J., Wilkin, J.L., Kohut, J., 2010. Highfrequency forcing and subtidal response of the Hudson River plume. J. Geophys. Res. 115 (C07), 012.

Hyder, P., Simpson, J., Christopoulos, S., 2002. Sea-breeze forced diurnal surface currents in the Thermaikos Gulf, North-west Aegean. Cont. Shelf Res. 22 (4), 585–601. http://dx.doi.org/10.1016/S0278-4343(01)00080-2.

IMR, 1977. Cruise Report (1) of R/V Dr. Fridtjof Nansen. Joint NORAD/Moçambique/FAO Project To Investigate the Fish Resources Off the Coast of Moçambique. Tech. rep. Institute of Marine Research.

IMR, 1978a. Cruise Report (3) of R/V Dr. Fridtjof Nansen, January-1978. Joint NORAD/Moçambique/FAO Project To Investigate the Fish Resources Off the Coast of Moçambique. Tech. rep. Institute of Marine Research.

IMR, 1978b. Cruise Report (4) of R/V Dr. Fridtjof Nansen, April-1978. Joint NORAD/Moçambique/FAO Project To Investigate the Fish Resources Off the Coast of Moçambique. Tech. rep. Institute of Marine Research.

Isobe, A., 2005. The ballooning of river-plume bulge and its stabilization by tidal currents. J. Phys. Oceanogr. 35, 2337–2351. http://dx.doi.org/10.1175/JPO2837.1.

Jurisa, J.T., Chant, R.J., 2013. Impact of offshore winds on a buoyant river plume system. J. Phys. Oceanogr. 43, 2571–2587. http://dx.doi.org/10.1175/JPO-D-12-0118.1.

Jury, M.R., Parker, B., Waliser, D., 1994. Evolution and variability of the ITCZ in the SW Indian ocean: 1988-90. Theor. Appl. Climatol. 48, 187–194. http://dx.doi.org/10.1007/BF00867048.

Kampf, J., 2009. Ocean Modelling for Beginners. Springer.

Kourafalou, V.H., Lee, T.N., Oey, L.-Y., Wang, J.D., 1996a. The fate of river discharge on the continental shelf. 2: Transport of coastal low-salinity waters under realistic wind and tidal forcing. J. Geophys. Res. 101 (C2), 3435–3455. http://dx.doi.org/10.1029/95JC03025.

Kourafalou, V.H., Oey, L.-Y., Wang, J.D., Lee, T.N., 1996b. The fate of river discharge on the continental shelf. 1: Modelling the river plume and the inner shelf coastal current. Geophys. Res. 101 (C2), 3415–3434.

Large, W.G., McWilliams, J.C., Doney, S.C., 1994. Oceanic vertical mixing: A review and a model with a nonlocal boundary layer parameterization. Rev. Geophys. 32 (4), 363–403. http://dx.doi.org/10.1029/94RG01872.

Lentz, S.J., Largier, J., 2006. The influence of wind forcing on the Chesapeake bay buoyant coastal current. J. Phys. Oceanogr. 36 (7), 1305–1316. http://dx.doi.org/10.1175/JPO2909.1.

Li, X., Chao, Y., McWilliams, J.C., Fu, L.-L., 2001. A comparison of two vertical-mixing schemes in a Pacific ocean general circulation model. J. Clim. 14, 1377–1398. http://dx.doi.org/10.1175/1520-0442(2001)014{\T1\textexclamdown}1377:ACOTVM{\T1\textquestiondown}2.0.CO;2.

Li, Y., Ning Chen, Y., Na Ruan, M., Wei Chen, J., 2015. The Jiulong river plume as cross-strait exporter and along-strait barrier for suspended sediment: Evidence from the endmember analysis of in-situ particle size, Estuarine. Coastal 759 Shelf Sci. 166 (PartB), 146–152.

Li, M., Zhong, L., Boicourt, W.C., 2005. Simulations of chesapeake bay estuary: sensitivity to turbulence mixing parameterization and comparison with observations. J. Geophys. Res. 110 (C12), http://dx.doi.org/10.1029/2004JC002585, 004.

Lutjeharms, J., 2006. The Coastal Oceans of South-Eastern Africa, in the Sea, 14B, Robinson, A. and Brink, K. Harvard University Press, Cambridge, MA, pp. 783–834.

Malauene, B.S., 2010. Shelf Edge Upwelling Off Northern Mozambique (Master's thesis). University of Cape Town, South Africa.

Mann, K.H., Lazier, J.R.N., 2006. Dynamics of Marine Ecosystems – Biological Physical Interactions in the Oceans, third ed. MA & Oxford: Blackwell Publishing, UK, http://dx.doi.org/10.5670/oceanog.2006.87.

Maúre, G.A., 2013. Effects of Biomass-Burning Aerosol Loading on Southern African Climate (Ph.D. thesis). University of Cape Town.

Mestres, M., Sierra, J.P., Sanchez-Arcilla, A., 2007. Factors influencing the spreading of a low-discharge river plume. Cont. Shelf Res. 27, 2116–2134. http://dx.doi.org/10.1016/j.csr.2007.05.008.

Moffat, C., Lentz, S.J., 2012. On the response of a buoyant plume to downwelling-favorable wind stress. J. Phys. Oceanogr. 42, 1083–1098.

Munchow, A., Garvine, R.W., 1993. Buoyancy and wind forcing of a coastal current. J. Mar. Res. 51, 293–322. http://dx.doi.org/10.1357/0022240933223747.

Nehama, F.P., 2012. Modelling the Zambezi River Plume using the Regional Oceanic Modelling System (Ph.D. thesis). University of Cape Town, RSA.

Nehama, F.P., Lemos, M.A., Machaieie, H.A., 2015. Water mass characteristics in a shallow bank highly influenced by river discharges: the Sofala Bank in Mozambique. J. Integr. Coastal Zone Manag. 15 (4), 523–532. http://dx.doi.org/10.5894/rgci560.

Nehama, F.P., Reason, C.J.C., 2014. Morphology of the zambezi river plume in the Sofala Bank, Mozambique. West. Indian Ocean J. Mar. Sci. 13 (1), 1–10.

Nehama, F.P., Reason, C.J.C., 2015. Modelling the Zambezi 781 river plume. Afr. J. Mar. Sci. 37 (4), 593–604. http://dx.doi.org/10.2989/1814232X.2015.1113202.

Oey, L.-Y., Mellor, G.L., 1993. Subtidal variability of estuarine outflow, plume, and coastal current: A model study. J. Phys. Oceanogr. 23, 164–171.

Pimenta, F.M., Campos, E.J.D., L.Miller, J., Piola, A.R., 2005. A numerical study of the plata river plume along the southeastern south American continental shelf. Braz. J. Oceanogr. 53 (3/4), 129–146. http://dx.doi.org/10.1590/S1679-87592005000200004.

Pinones, A., Valle-Levinson, A., Narvaez, D.A., Vargas, C.A., Navarrete, S.A., Yuras, G., Castilla, J., 2005. Wind-induced diurnal variability in river plume motion. Estuar. Coast. Shelf Sci. 65, 513–525. http://dx.doi.org/10.1016/j.ecss.2005.06.016.

Sætre, R., 1985. Surface currents in the Mozambique channel. Deep-Sea Res. 32 (12), 1457–1467. http://dx.doi.org/10.1016/0198-0149(85)90097-4.

Sætre, R., da Silva, J., 1982. Water masses and circulation on the mozambique channel. Revista de InvestigaÇãO Pesqueira 3–38.

Shchepetkin, A.F., McWilliams, J.C., 2005. The regional oceanic modeling system (ROMS): a split-explicit, free-surface, topography-following-coordinate oceanic model. Ocean Model. 9 (4), 347–407. http://dx.doi.org/10.1016/j.ocemod.2004.08.002.

Sheng, J., 2001. Dynamics of a buoyancy-driven coastal jet: the Gaspé Current. J. Phys. Oceanogr. 31, 3146–3162.

Siddorn, J.R., Bowers, D.G., Hoguane, A.M., 2001. Detecting the Zambezi river plume using observed optical properties. Mar. Pollut. Bull. 42 (10), 942–950. http://dx.doi.org/10.1016/S0025-326X(01)00053-4.

Stumpf, R.P., Gelfenbaum, G., Pennock, J.R., 1993. Wind and tidal forcing of a buoyant plume, mobile bay, Alabama. Cont. Shelf Res. 13 (11), 1281–1301. http://dx.doi.org/10.1016/0278-8044343(93)90053-z.

Tinley, K., 1971. Determinants of coastal conservation dynamic and diversity of the environment as exemplified by the Moçambique coast. In: Symposium on nature conservation as a form of land use - Gorongosa National Park, pp. 125–153.

Warrick, J.A., DiGiacomo, P.M., Weisberg, S.B., Nezlin, N.P., Mengel, M., Jones, B.H., Ohlmann, J.C., Washburn, L., Terrill, E.J., Farnsworth, K.L., 2007. River plume patterns and dynamics within the Southern California Bight. Cont. Shelf Res. 27, 2427–2448. http://dx.doi.org/10.1016/j.csr.2007.06.015.

Warrick, J.A., Mertes, L.A.K., Washburn, L., Siegel, D., 2004a. A conceptual model for river water and sediment dispersal in the Santa Barbara Channel, California. Cont. Shelf Res. 24, 2029–2043. http://dx.doi.org/10.1016/j.csr.2004.07.010.

Warrick, J.A., Mertes, L.A.K., Washburn, L., Siegel, D., 2004b. Dispersal forcing of southern california river plumes, based on field and remote sensing observations. Geo-Marine Lett. 24, 46–52. http://dx.doi.org/10.1007/s00367-003-0163-9.

Warrick, J.A., Stevens, A.W., 2011. A buoyant plume adjacent to a headland - observations of the Elwha river plume. Cont. Shelf Res. 31, 85–97. http://dx.doi.org/10.1016/j.csr.2010.11.007.

Xia, M., Xie, L., Pietrafesa, L.J., 2007. Modeling the cape fear river estuary plume. Est. Coasts 30 (4), 698–709. http://dx.doi.org/10.1007/BF02841966.